conference pre-print

OVERVIEW OF WENDELSTEIN 7-X HIGH-PERFORMANCE OPERATION

O. Grulke and the Wendelstein 7-X Team Max Planck Institute for Plasma Physics Greifswald, Germany Email: olaf.grulke@ipp.mpg.de

Abstract

After

1. INTRODUCTION

The Wendelstein 7-X (W7-X) stellarator has recently completed two experimental campaigns, OP 2.2 and OP 2.3, carried out over the last two years. These campaigns marked the first implementation of a revised operational strategy, designed to maximize experimental efficiency by reducing commissioning overhead. Instead of conducting a full time consuming recommissioning before each phase, a single commissioning period preceded two full three-month experimental campaigns. The basic elements of the operation schedule is depicted in Fig. 1. Between phases, a short maintenance phase is introduced, however neither the cryogenic system was warmed up

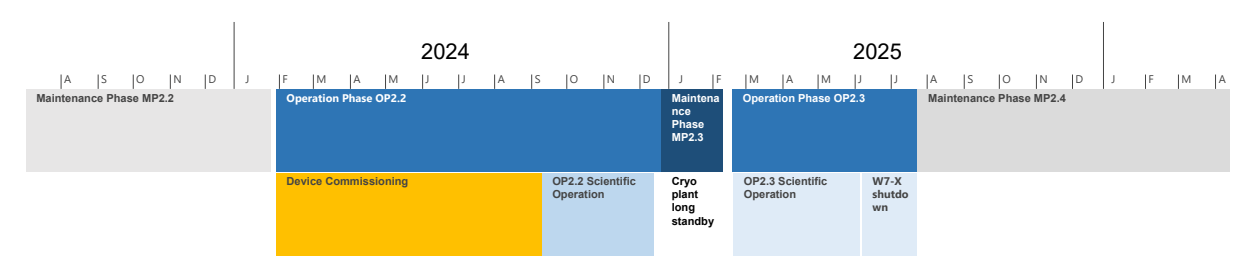


FIG. 1. W7-X operation schedule in 2024 and 2025.

nor the plasma vessel vented, thereby enabling a direct transition between operational periods. This approach required comprehensive scientific planning and placed high demands on the technical reliability of the device and exceptional performance from key subsystems, which need to be in full operation for longer than one year. The W7-X components demonstrated reliability well beyond expectations, with failure rates below 1%. This stability was crucial for supporting long campaign durations and consistent experimental conditions. Plasma operation was carried out in both campaigns without major issues. Typically, 80-100 scientific discharges were performed per day across a broad range of magnetic field configurations, representing an improvement also in terms of execution efficiency. Several major technical upgrades were implemented prior to OP 2.2 to further strengthen operational capabilities. These included the prototype operation of a high-power gyrotron (1.3 MW steady-state at a frequency of $f = 140 \,\mathrm{GHz}$) [1], the installation of a steady-state pellet injector, improvements to multiple diagnostic systems, and enhancements of plasma feedback control systems. The latter incorporated radiation feedback, electron cyclotron resonance heating (ECRH) power stabilization, and plasma density control via ECRH. The scientific program of OP 2.2 and OP 2.3 was directed toward high-performance plasma operation. Key objectives included the extension of discharge duration, improvement of plasma confinement, and exploration of high-beta regimes. Complementary studies addressed power exhaust, with detailed investigations of the scrape-off layer (SOL) and divertor heat loads, in particular the influence of drift effects on divertor strike-line patterns. Together, these campaigns advanced both the technical and scientific basis of W7-X, consolidating its role as the leading device for steady-state stellarator research. The paper is organized as follows: In Sec. 2 the key enhancements are introduced. Sec. 3 outlines the progress of longe-pulse operation, before the key findings of operation at high plasma- β in Sec. 4, improved confinements in Sec. 5, and divertor heat load studies in Sec. 6 are summarized.

2. ENHANCEMENTS AND OPERATION OVERVIEW

In preparation for future high-performance, steady-state operation, W7-X has initiated a comprehensive upgrade strategy aimed at enhancing both plasma heating capabilities and particle fueling systems. These developments are critical to supporting plasma discharges lasting up to 30 minutes at elevated performance levels. The extension of plasma heating power follows a dual approach, targeting upgrades to both the neutral beam injection (NBI) and electron cyclotron resonance heating (ECRH) systems over the coming years. At the current stage, ECRH upgrades focus on the deployment of high-power gyrotrons up to a power of 2 MW capable of delivering increased reliable steady-state power levels of at least 1 MW. A first prototype of a 1.5-MW-Class gyrotron has been has been successfully operated during the last two experimental campaigns. Compared to the original design of the 1-MW W7-X gyrotrons, the upgraded tube incorporates a resonator with a larger diameter and operates in the $TE_{28,10}$ mode. Together with the improved cooling systems, this enables enhanced power loading on internal gyrotron components. As shown in Fig. 2, which presents a photograph of the gyrotron alongside power measurements on a matched test load, the output power is limeted to 1.3 MW by the onset of parasitic oscilations near 122.5 GHz and 135 GHz. These oscillations degrade the electron beam quality, reducing beam-wave interaction efficiency and generating additional intrinsic stray radiation within the gyrotron. As a countermeasure, the next gyrotron will have an improved beam tunnel. During plasma operation, the gyrotron was routinely operated at an output power of 1.1 MW without any issues.

In parallel with heating system enhancements, a new screw-type pellet injector has been developed to meet the demanding particle fueling requirements of long-pulse operation [2]. This injector is capable of delivering hydrogen or deuterium pellets with variable diameters ranging from 2 mm to 3 mm. The injection velocity can be precisely controlled within the range of 400–600 m/s, and the system supports repetition rates of up to 5 Hz. The design emphasizes compatibility with W7-X's long-pulse mission by enabling continuous operation over extended discharge durations of up to 30 minutes. This is achieved through a robust drive mechanism and active cooling of critical components, ensuring thermal and mechanical stability during prolonged use. Due to the injector's flexibility in pellet size and injection parameters, it is planned to integrate the pellet fueling into the real-time peak density control system in the near future. While feedback systems are not fundamentally required for plasma control in stellarators due to their intrinsic steady-state magnetic configurations, W7-X has significantly enhanced its feedback control capabilities to enable precise and reproducible scientific and long-pulse operation. A new feedback control system has been implemented to regulate total plasma radiation by actively controlling impurity seeding rates. The system utilizes measurements from the bolometry diagnostic to assess total radiated power and adjusts the seeding gas injection accordingly to maintain a desired radiation level. Figure 3a) illustrates a representative discharge in which the target radiation level is increased in a stepwise fashion from 3.5 MW to 6.2 MW. Neon was used as the seeding gas, and the feedback system modulated the valve voltage to achieve each desired radiation level. The agreement between the target and measured radiation is excellent, demonstrating the system's effectiveness. This capability has been employed both scientifically for studies of impurity-seeded detachment and operationally, to reduce localized power loads on divertor target plates during long-pulse discharges.

Operational experience from earlier W7-X campaigns revealed that long-pulse discharges at elevated ECRH



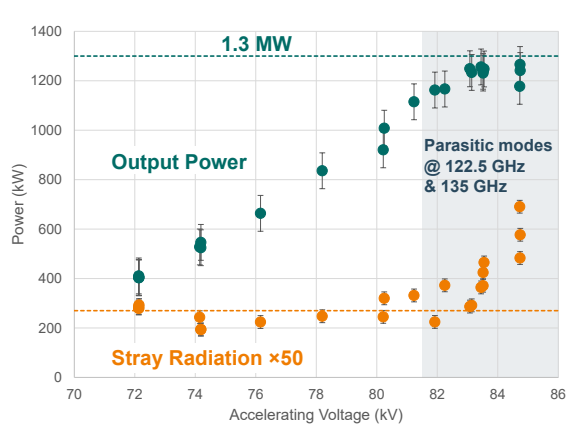


FIG. 2. Photograph of the new 1.5 MW gyrotron in its final location (left) and measurement of the gyrotron output power onto a test load vs. its acceleration voltage.

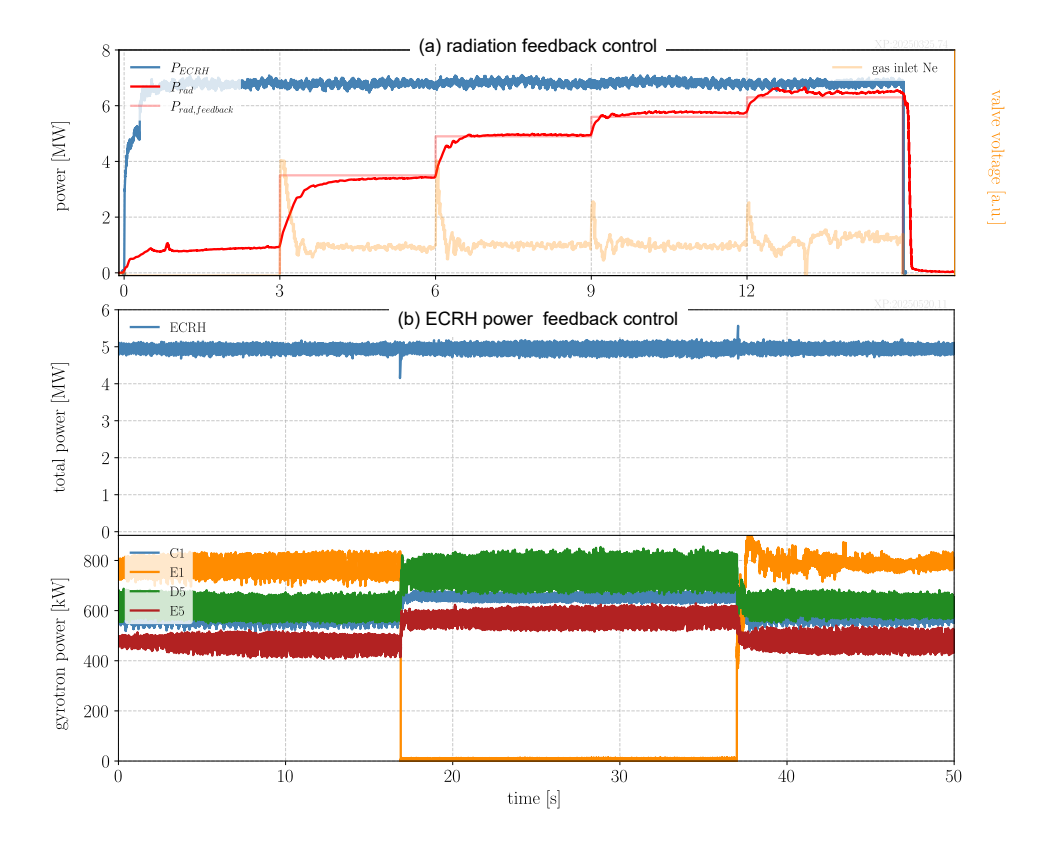


FIG. 3. Examples of newly established feedback control systems: (a) Seeded radiation feedback control, (b) ECRH power stabilization feedback control.

power levels are occasionally interrupted by spontaneous failure of individual gyrotrons. These unanticipated power losses lead to undesired variations of the operation parameters. To address this, a new ECRH power stabilization system was implemented. When a gyrotron trips, the system compensates in real time by increasing the output power of the remaining operational gyrotrons, thereby stabilizing the total injected ECRH power. Figure 3b shows an example of this stabilization strategy for a subset of gyrotrons. In the illustrated case, gyrotron E1 experiences a temporary dropout during the time interval $t=17-36\,\mathrm{s}$. In response, the power outputs of the remaining gyrotrons are increased accordingly, successfully maintaining a constant total heating power throughout the dropout period. This approach ensures uninterrupted plasma heating and enhances the robustness of long-pulse operation.

3. LONG PULSE OPERATION

W7-X is designed for long-pulse operation with plasma discharges of up to 30 min duration and a total heating energy of 18 GJ. This is facilitated by the superconducting magnetic field coils and water-cooled plasma-facing components (PFC). However, the development of localized hot spots and potential leading edges can cause excessive heat fluxes, particularly at the divertor, which may exceed its design specifications. For this reason, a step-wise operational approach has been pursued: during campaign OP 2.1, a heating energy of 1.3 GJ was successfully reached [3]. This specification value was increased to 2 GJ during the last campaigns OP 2.2 and OP 2.3, with the intention of gradually approaching the design limits in the upcoming operation campaigns. A steadystate scenario was developed with the potential for further increases in heating energy and consists of several elements: To mitigate convective heat loads on the PFCs, the divertor was operated in a detached state, achieved via feedback-controlled impurity seeding. The electron cyclotron resonance heating (ECRH) was applied in X2 polarization, which provides excellent single-pass absorption and prevents from ECRH power deposition on the beam dump. To stabilize the strike line position on the divertor, counter-electron cyclotron current drive (ECCD) was employed, thereby compensating the bootstrap current and maintaining a small net toroidal current. Figure 4 shows time traces of the ECR heating power, plasma radiation power, and plasma density. A discharge length of 363 s was achieved with nearly constant heating and radiation power levels. The plasma density, regulated via feedback control, remained constant throughout the discharge. The constant ECRH power was the result of successful power stabilization feedback. Although sporadic gyrotron dropouts occurred during the pulse, these were

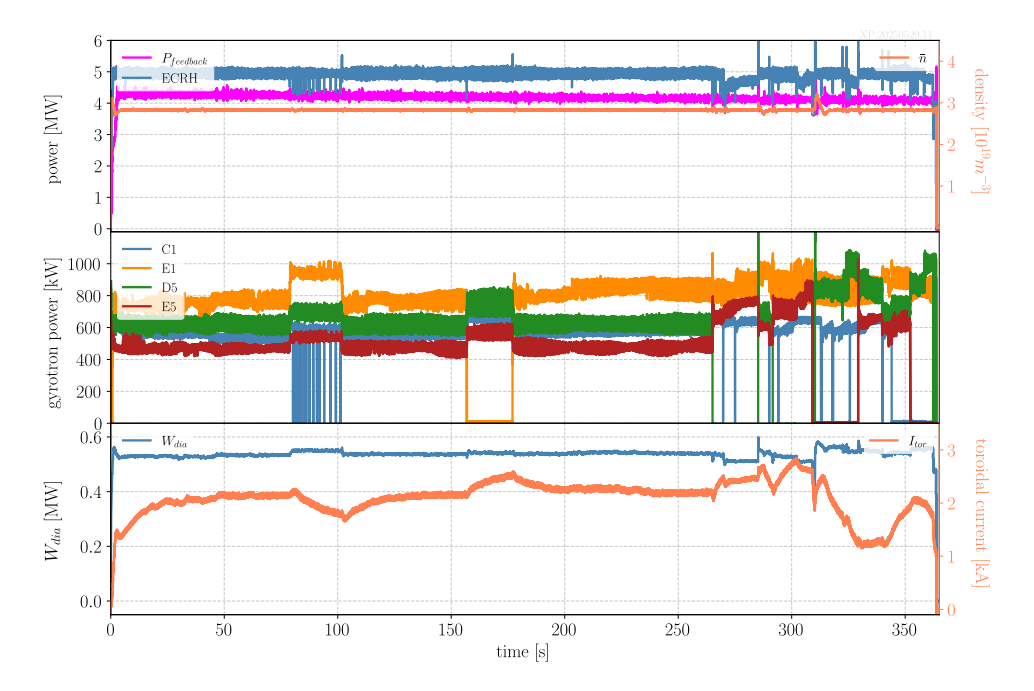


FIG. 4. Overview of long-pulse operation reaching a total energy turnaround of 1.8 GJ. Shown are time traces of the total ECR heating power together with the feedback-controlled radiation power and mean plasma density (top), a selection of individual gyrotron power levels (middle), and the achieved diamagnetic energy and total toroidal current (bottom).

compensated by corresponding increases in power from other gyrotrons. The diamagnetic energy W_{dia} remained steady, while the toroidal plasma current was consistently maintained below 3 kA. Beginning at $t=270\,\mathrm{s}$, strong fluctuations in the power of individual gyrotrons were observed. These fluctuations became increasingly frequent and ultimately led to the termination of the discharge at 363 s. At this point, a total heating energy of 1.8 GJ had been achieved. Despite the premature termination of the discharge, the developed scenario was successful in maintaining low PFC heat fluxes and convective divertor loads below $3.5\,\mathrm{MW/m^2}$. The observed fluctuations in gyrotron power were traced back to cooling issues in the ECRH beamline, which caused elevated component and air temperatures. This led to an increasing rate of arcing events in the ECRH beamline and ultimately to the discharge termination. For the upcoming campaign, improvements to the cooling system are planned to prevent a recurrence of this limitation.

4. OPERATION AT HIGH PLASMA- β

W7-X is designed for improved magnetohydrodynamic (MHD) stability at high plasma- β , with target values up to 4%, consistent with reactor requirements of the HELIAS line [4, 5]. In this context, the confinement of energetic ions, which mimic α -particle behavior in a stellarator reactor, is a crucial performance metric. Numerical simulations predict that fast ion losses increase strongly with rising plasma- β [6]. Demonstrating high- β operation is therefore an important step toward reactor-relevant validation. From fundamental confinement scaling arguments, achieving such conditions would require very high heating powers, which are not available at W7-X. However, according to the ISS04 stellarator confinement scaling, the dependence of the confinement on magnetic field strength is weaker than on plasma β . This insight allows high- β operation to be made accessible by reducing the magnetic field strength, thereby relaxing the heating power requirements. The primary heating system at W7-X is the electron cyclotron resonance heating (ECRH) system at 140 GHz, which can be also applied in X3 polarization at a magnetic field of $B=1.7\,\mathrm{T}$. However, direct plasma startup using X3 polarization is not feasible: the single-pass absorption is negligible for electron temperatures $T_e < 1\,\mathrm{keV}$, since the absorption power scales approximately as $P_{abs} \sim nT_e^2$ [7]. To overcome this, a discharge startup scheme was developed employing ECRH at 101 GHz in X2, technically limited to a short pulse, as shown in Fig. 5. The initial ECRH pulse generates a plasma with density $n \approx 1 \cdot 10^{19} \, \mathrm{m}^{-3}$, which is sufficient for reasonable neutral beam injection (NBI) absorption. Subsequently, typically two NBI sources with a combined heating power of $P_{NBI} = 3.6 \,\mathrm{MW}$ are applied, leading to increased plasma density and, crucially, higher electron temperatures. Once adequate conditions are established, the remaining ECRH power in X3 polarization can take over the heating from NBI, thereby sustaining

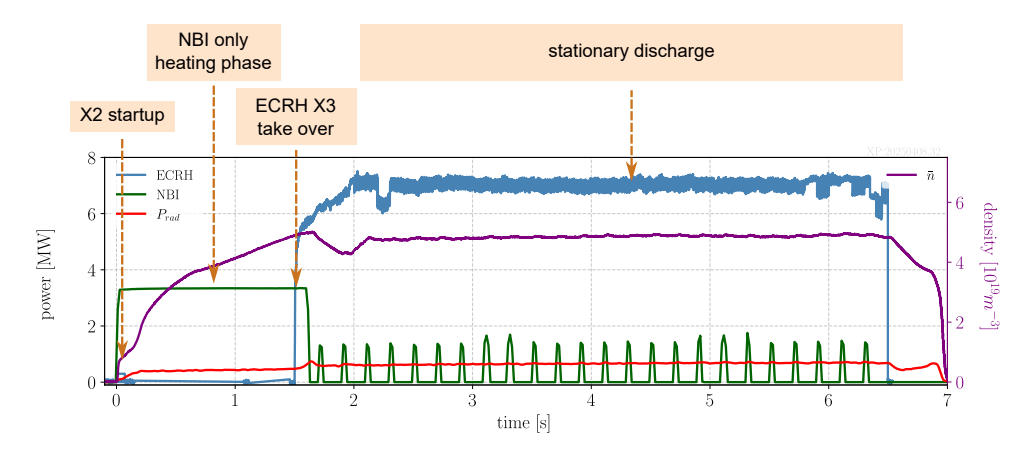


FIG. 5. Demonstration of plasma operation at reduced field with ECR heating in X3 polarization. Shown are the time traces of the ECR and NBI heating powers together with the mean plasma density. The different phases of the discharge - startup, NBI heating, and X3 takeover - are indicated.

and extending the discharge. This scheme was successfully demonstrated at W7-X, enabling stable plasma operation up to 6.5 s. Because of the incomplete single-pass absorption of X3 polarization, a triple beampath scheme with the established O2-reflector tiles was used for the first experiments in OP2.2/2.3, illustrated in Fig. 6. In contrast to O2 heating, which exhibits strong absorption at incidence angles of $10^{\circ} - 20^{\circ}$ to the magnetic field, X3 heating is most efficient at perpendicular incidence, but at medium densities also safely operable with oblique incidence. This configuration effectively increases the absorption path length, enabling nearly complete absorption of the injected ECRH power and thus efficient plasma heating under reduced magnetic field conditions. A dedicated multipass scenario with customized reflector tiles is in preparation for OP2.4. It must be noted that the frequency limitations of the short-pulse gyrotron to $f \geq 101\,\mathrm{GHz}$ does not match the cold X3 resonance, which is for a magnetic field of $B \approx 1.7 \, \text{T}$. Thus, a non-zero plasma- β is required to reduce the central magnetic field and allow X3 absorption on the magnetic axis. This optimized discharge scheme yields the presently highest peak and volume-averaged plasma-\beta achieved in W7-X. The representative discharge is illustrated in Fig. 7 and closely follows the scheme described above. After $t=2\,\mathrm{s}$, the X3 heating phase commences, driving the plasma to exceptionally high ion temperatures, with transient values reaching $T_i \gtrsim 3\,\mathrm{keV}$. It is noteworthy that already during the preceding NBI heating phase, the radial plasma- β profile develops distinct gradients, which continue to steepen as the discharge evolves. This progressive shaping is clearly reflected in the radial profile of local plasma- β values, which start at approximately $\beta \approx 1\%$ in the early phase and subsequently rise to centrally

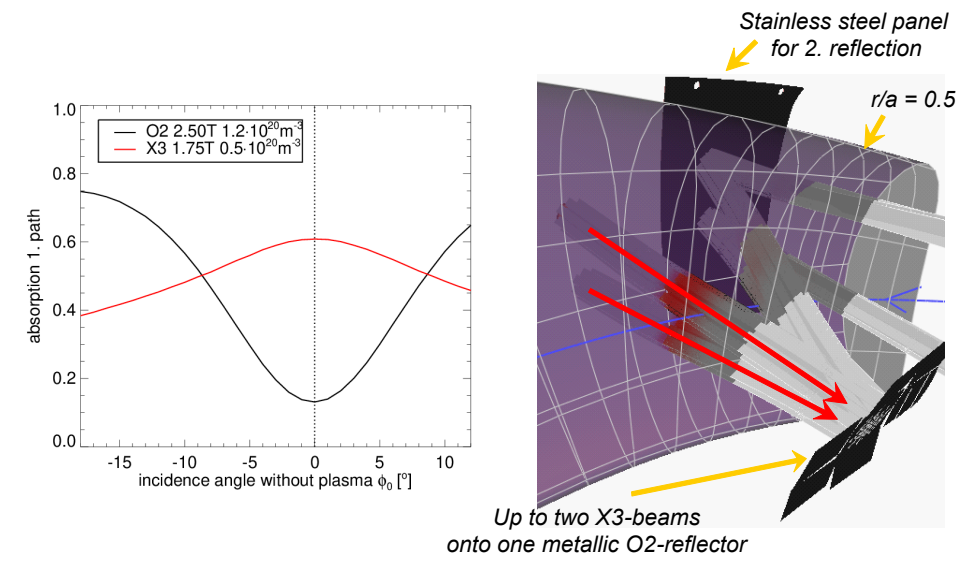


FIG. 6. (left) Comparison of the dependence of ECRH absorption on incidence angle between O2 polarization at a magnetic field of $B=2.5\,T$ and X3 polarization at $B=1.75\,T$. (right) Schematic of the ECRH heating beam paths. The beams are entering along the red arrows.

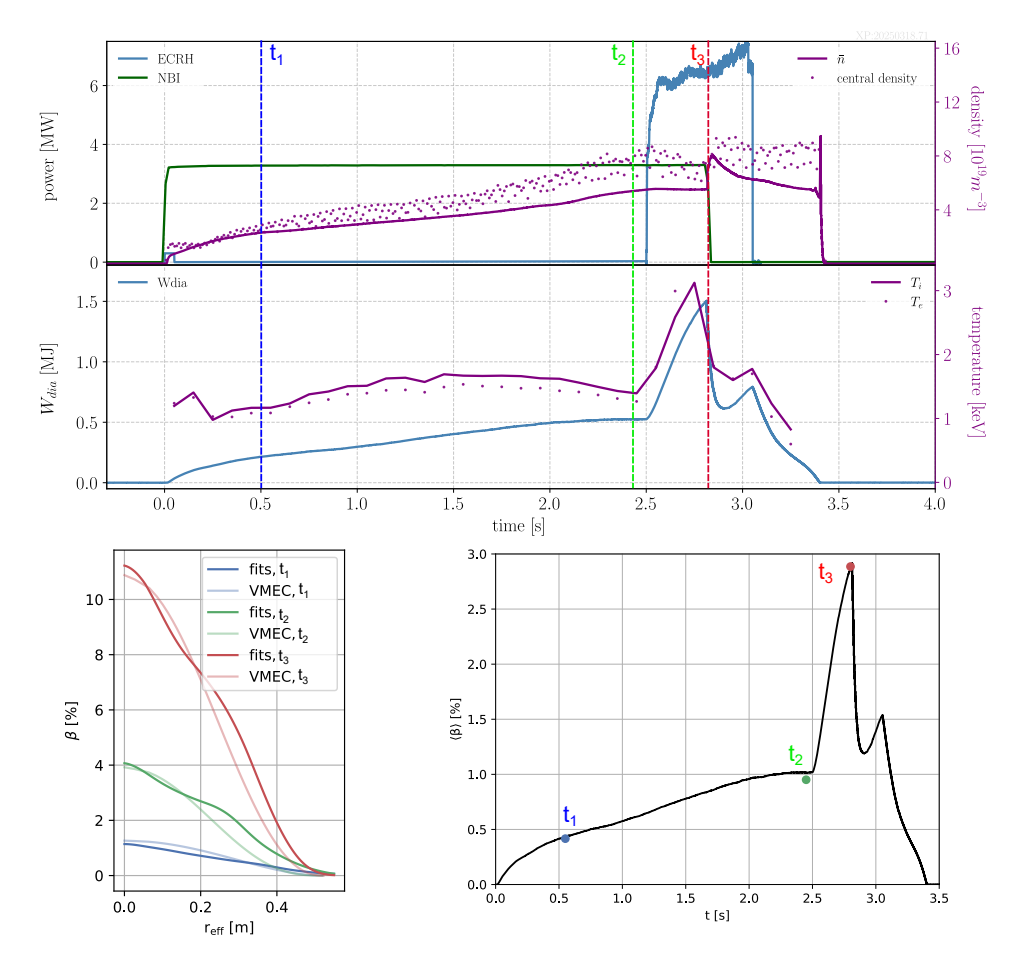


FIG. 7. Low-field discharge (top), derived profiles of plasma- β from profile diagnostics and equilibrium reconstructions for three characteristic time instants $t_1 - t_3$, and the respective achieved volume-averaged plasma- β .

peaked values exceeding $\beta>10\%$ during the X3 heating period. The influence of the elevated β values on the magnetic equilibrium has been assessed using the VMEC code, which confirms significant modifications of the radial magnetic field structure. The strongly peaked central profile is identified as a decisive factor in enabling these high β values (cf. Sec. 5). The high central plasma- β translates into an equally remarkable increase in the volume-averaged quantity $\langle \beta \rangle$, which rises from $\langle \beta \rangle = 0.5\%$ in the early phase to $\langle \beta \rangle = 2.8\%$ at the peak of the discharge. This represents the highest $\langle \beta \rangle$ value obtained in W7-X to date and highlights the importance of operating at reduced magnetic field to access high plasma- β regimes for studies of MHD stability limits and validate fast ion confinement predictions.

5. HIGH-PERFORMANCE OPERATION AND ADVANCED HEATING SCENARIOS

Previous operation campaigns of Wendelstein 7-X (W7-X) have provided clear evidence that plasma confinement can be improved in discharge scenarios that employ a central peaking of the radial plasma density profile [8]. This effect directly contributed to the achievement of record values of the fusion triple product in stellarator devices [9]. In these discharges, central density fueling was realized by pellet injection, which provided a localized source of particles deep in the plasma core. More recently, first indications were obtained that central density peaking can also be established using neutral beam injection (NBI) [10]. In this case, the resulting centrally peaked density profile is not solely a consequence of direct NBI particle fueling. Rather, after the initial fueling phase, radial particle transport is found to be significantly reduced, thereby supporting and maintaining the central peaking of the density distribution [11]. This marks an important step in broadening the operational flexibility of W7-X toward confinement-optimized scenarios. In the most recent campaigns, further detailed studies were conducted to tailor discharge conditions specifically toward maximizing plasma confinement and performance. Two conceptually distinct approaches were pursued: (i) discharges in which NBI heating facilitates the formation and stabilization of centrally peaked density profiles, and (ii) discharges relying on central density fueling via pellet injection. These complementary schemes provide a valuable experimental basis for understanding the interplay

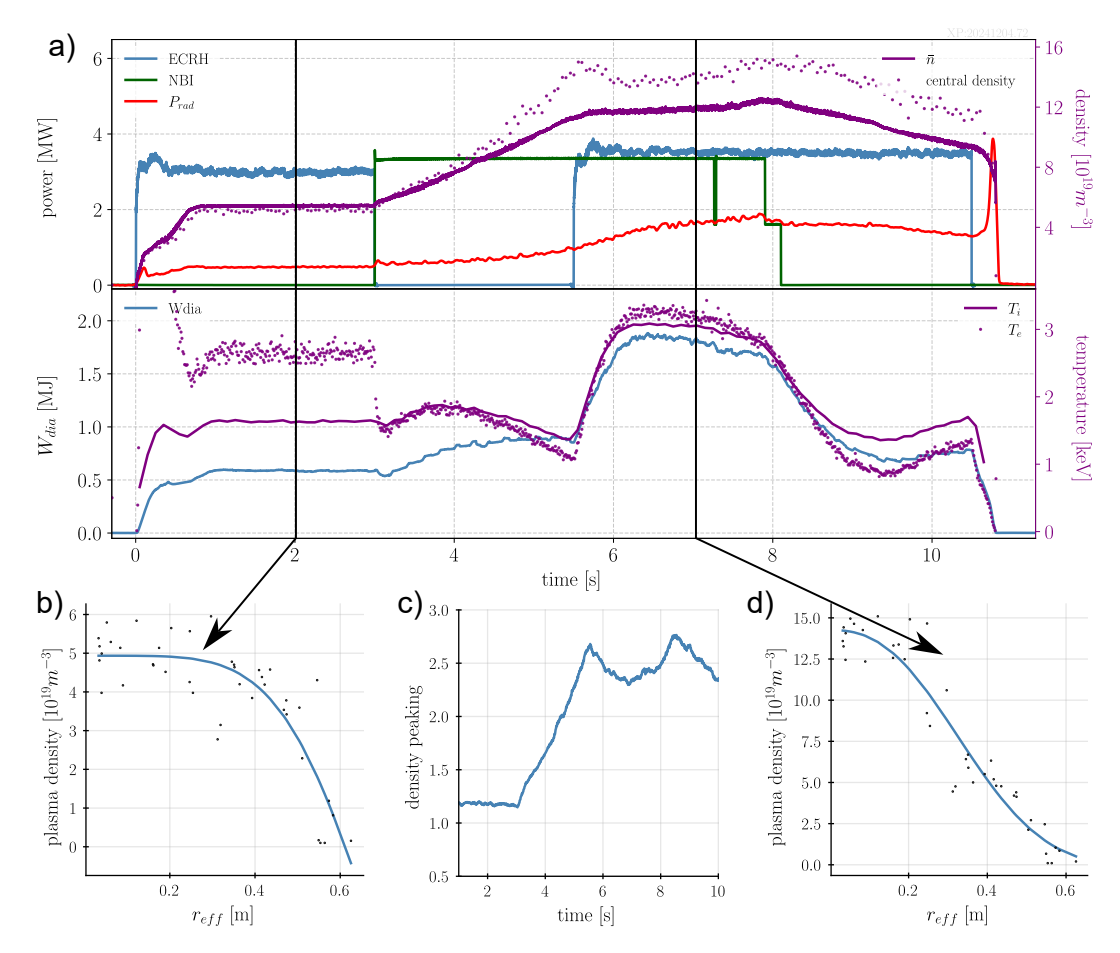


FIG. 8. Discharge scenario of record fusion triple products for stellarators. The top graph a) shows time traces of the ECRH and NBI heating powers together with the total radiated power P_{rad} , mean \bar{n} and central plasma density traces (top), and the diamagnetic energy W_{dia} and central electron T_e and ion temperatures T_i . For two instants, the radial density profiles are shown in b) and d). As a measure of the density profile evolution, the time trace of the ratio of core to edge (r/a = 0.8) density is shown in c), denoted as peaking.

between fueling methods, radial transport processes, and overall stellarator confinement optimization. The typical discharge scenario for NBI-heating-induced central density peaking is illustrated in Fig. 8. It begins with an ECRH plasma initiated in X2 polarization at moderate heating powers and densities. The corresponding plasma density profile, shown in Fig. 8 at t=2 s, is centrally flat and exhibits radial density gradients only in the outer region at $r_{eff} > 0.3 \, \mathrm{m}$. A key step for establishing central density peaking is the transition of plasma heating entirely to NBI, without any additional ECRH. In this phase, the absence of central electron heating leads to equilibrated electron and ion temperatures, albeit at relatively low ion temperature levels. During the initial NBI fueling phase, the plasma density increases over several seconds before a distinct peaking of the density profile emerges in the plasma core. Once the profile is peaked, ECRH is re-applied to provide additional plasma heating. With the added power, the electron and ion temperatures, as well as the diamagnetic energy, rise rapidly and subsequently saturate at a stationary level, which in the present case persists for approximately two seconds. In this regime, the radial density profile remains strongly peaked in the plasma center with significant gradients already at $r_{eff} > 0.1$ m. The density peaking factor, defined as $p = n_{core}/n_{r/a=0.8}$, exhibits a gradual increase during the NBI heating phase before saturating at values of $p \approx 2.5$. The stationary phase of elevated temperatures and stored energy is sustained as long as NBI heating is applied, which is currently limited by the maximum available NBI pulse length. The peak ion temperature reaches $T_i \approx 3 \, \text{keV}$, in good agreement with what is expected from neoclassical ion heat transport [8]. This indicates that transport in this regime is strongly dominated by neoclassical processes, in contrast to flat-density profiles where turbulent transport remains the dominant mechanism. In the high temperature phase, the energy confinement exceeds the ISS04 scaling by typically 30-40%. It should be noted that there is a power limit of ECRH in these kind of scenarios, from which on the central plasma density peaking is strongly reduced due to ECRH density pump out.

The duration of the improved confinement phase has so far been primarily limited primarily by the operational

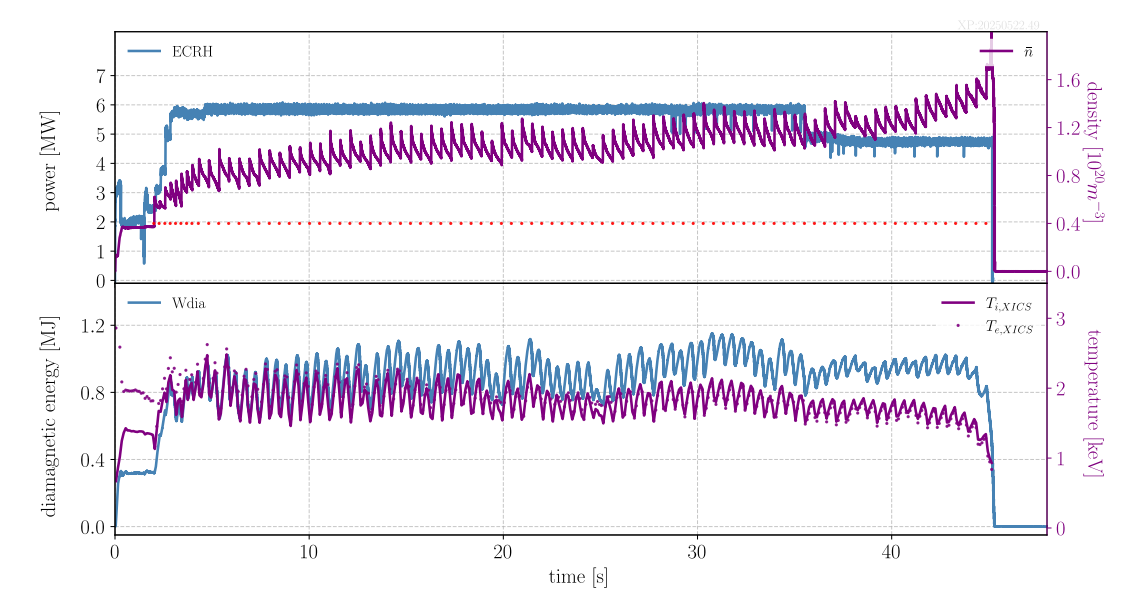


FIG. 9. Example of a long-pulse high performance discharge initiated and maintained by pellet injection only. The red dots in the top graph denote the time instants of pellet injection.

time of the NBI system. A promising strategy to extend this phase is to initiate radial density peaking through a sequence of pellet injections, which can then be maintained by subsequent NBI heating, thereby yielding a noticeable prolongation of the improved confinement. To achieve sustainment over much longer timescales, however, the peaking must be supported by pellet injection alone. Such a scheme has already been demonstrated in earlier experiments [12], but only in a transient manner and for relatively short periods, as the previously available pellet injector was restricted to injection times of only a few seconds. With the recent availability of a new steady-state pellet injector, it is now possible to pursue this approach under substantially improved conditions, offering the prospect of sustaining the improved confinement phase for much longer durations and with greater experimental flexibility. The longest pellet-injection discharge to date is presented in Fig. 9. Following plasma start-up, pellet injection begins at t=2 s with an initial repetition frequency of 3.5 Hz, which is later reduced to 2 Hz during the discharge. The injection times of the individual pellets are indicated by red dots in Fig. 9. Owing to the high plasma densities, ECR heating is applied in O2 polarization, with a constant power of 6 MW until t = 35 s, when the power is stepped down. Each pellet induces a modulation of the plasma density; however, the average density remains relatively constant at $\bar{n} \approx 1.2 \cdot 10^{20}$, m⁻³. A slight upward trend in plasma density is nevertheless observed, which is mitigated by reducing the pellet injection frequency after 5s. The pellet injections in this experiment are executed in a feed-forward manner. The results strongly suggest that, for longer discharge scenarios, effective control of the density will require a feedback system with variable pellet injection frequencies to stabilize the temporal density evolution, which will be realized in the near future. This is especially visible in the later phases of the discharges with reduced ECR heating power, in which the pellet fueling leads to a steady increase of the plasma density. The achieved ion temperature values, although smaller than in the combined NBI and ECRH scenario shown in Fig. 8, partly due to the smaller plasma heating power, are still significantly enhanced on average by 25% compared to discharges with gas fueling at similar ECR heating power levels [8, 13]. The results of both scenarios—either improved plasma performance with combined ECRH and NBI, or through a sequence of pellet injections—consistently indicate a reduction of radial heat transport. This finding is further supported by a database study for W7-X, in which the turbulent heat flux Q_{anom} is evaluated as a function of $2n\nabla T_i$ at a given radius of r/a = 0.4, see Fig. 10(left) (extend from Ford et al. [10]. The normalized density gradient length a/L_n , with a denoting the minor plasma radius, is represented in a color scale. Two clearly distinct regimes emerge: for small normalized density gradients, the heat flux is large and originates from a significantly higher turbulent heat diffusivity, $\chi_{anom} \approx 1.2 \pm 0.5$, m²/s. Conversely, the turbulent heat flux is considerably reduced when the normalized density gradient length is increased, yielding typical values of the turbulent heat diffusivity smaller by about a factor of five, in the range $\chi_{anom} \approx 0.25 \pm 0.08$, m²/s. It has ben shown that this behavior is a feature of essentially all discharge scenarios with centrally peaked density profiles [14]. This grouping of heat flux persists even when a transition between both regimes occurs during a single discharge, for instance due to a loss of density profile peaking caused by ECRH-induced density pump-out. This result is consistent with the fundamental understanding of turbulent transport in W7-X. Both numerical simulations and experimental observations provide

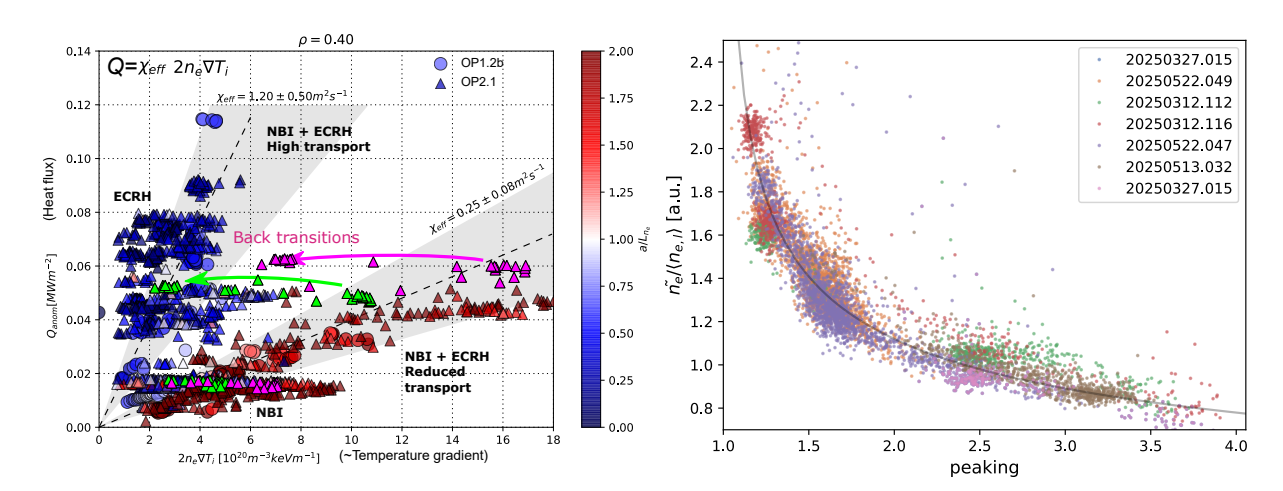


FIG. 10. (left) Database analysis of the anomalous heat flux versus ion temperature gradient. The color-code denotes the density gradient length normalized to the minor plasma radius a/L_n . The dashed lines with shaded intervals denote the effective ion heat diffusivity.(right) Compilation of discharges with improved confinement phases. Shown are the relative density fluctuation degree versus the density peaking.

compelling evidence that turbulent transport in W7-X is predominantly driven by ion temperature gradient (ITG) turbulence [16–19] in ECRH heated, gas-fueled discharge scnearios. In contrast, density-gradient-driven trapped electron mode (DTEM) transport is known to be strongly suppressed in the W7-X magnetic configuration which approaches maximum-J [20, 21], owing to the reduced regions of resonance between the diamagnetic drift and the precessional drift of trapped electrons. As a consequence, ITG turbulence in W7-X can be stabilized by density gradients without the concurrent destabilization of DTEMs, leading to improved energy confinement, elevated ion temperatures, and enhanced diamagnetic energies. This interpretation is further supported by the observed dependence of the density-normalized turbulent density fluctuation level on the degree of density profile peaking, Fig. 10(right). For a set of improved-confinement discharges — including the combined ECRH and NBI scenario as well as discharges with pellet-fueling-sustained density peaking — a clear anti-correlation is found between the

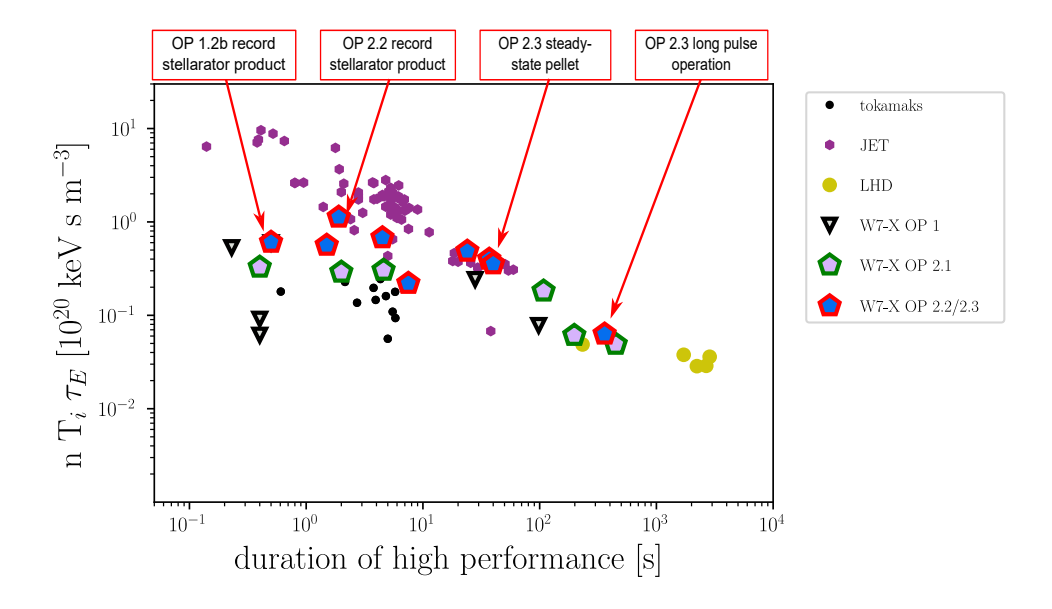


FIG. 11. Compilation of the fusion triple products [15] including the newest data from JET and the last two W7-X campaigns.

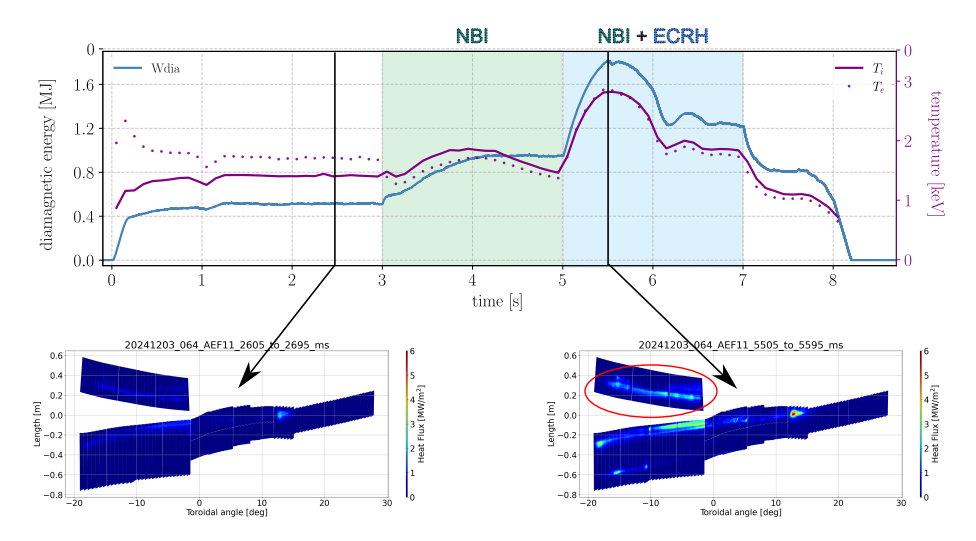


FIG. 12. Improved confinement discharge with combined ECRH and NBI heating together with heat flux calculations as derived from infrared surface temperature observations for two time instants of small and large plasma- β .

fluctuation level and the steepness of the density profile, expressed here as the ratio of central to edge (r/a=0.8) density. Density-normalized turbulence levels steeply drop when the density profile is peaked.

The improved-confinement discharges achieved in W7-X have led to unprecedented fusion triple products $nT_i\tau_E$ for stellarators. These results have been incorporated into the most recent CICLOP database and are presented in Fig. 11 [22]. Building on the first stellarator record for the triple product, obtained in W7-X during operational campaign OP 1.2b (2018) with pellet injection, the value was substantially increased in OP 2.2 (2024) in the combined ECRH and NBI scenario (cf. Fig. 8), reaching a maximum of $nT_i\tau_E = 1.126 \cdot 10^{20}$, keV, s, m⁻³. While these record values remain below those achieved in larger tokamaks, W7-X performance decreases by only about 50% under the continuous pellet-fueling scheme demonstrated in OP 2.3 (2025) (cf. Fig. 9). Importantly, the resulting triple product values are comparable to those of tokamaks, with the added potential of extending them to much longer durations in future campaigns.

6. DIVERTOR LOADS AND SCRAPE-OFF LAYER DRIFTS

W7-X is equipped with a novel, fully water-cooled island divertor that has been specifically engineered to enable steady-state, long-pulse operation [3]. The positioning of the strike lines on the divertor targets is governed primarily by the selected magnetic configuration and the corresponding edge rotational transform. However, plasma currents also play a non-negligible role, and it has been demonstrated that the bootstrap current can substantially modify the spatial distribution of power deposition across the divertor plates [23]. Equilibrium reconstructions

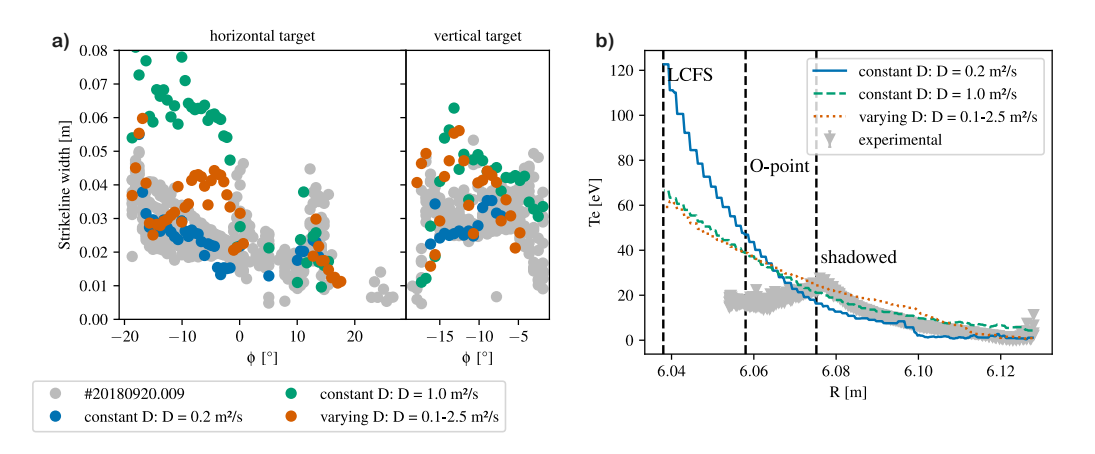


FIG. 13. EMC3 calculation of a) the widths of the divertor strike line on the horizontal and vertical target for variations of the perpendicular particle diffusivity D and b) for the same variations of D a comparison of calculations of the electron temperature T_e with measurements from probe diagnostics.

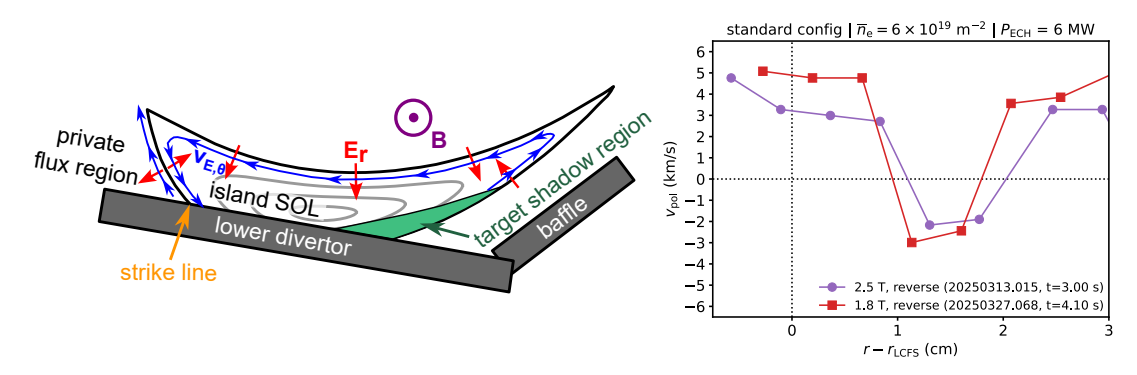


FIG. 14. (left) Schematic of poloidal (along the island flux surface) $E \times B$ flows resulting from the electric field distribution within an W7-X edge magnetic island. (right) Comparison of measurements of the flow velocity for two different magnetic field strength $B=2.5\,T$ and $B=1.8\,T$.

carried out with the HINT code further extend this understanding by predicting that, in high- β plasmas, the geometry of the magnetic islands is changed such that magnetic connection between the separatrix and the divertor target plates is modified [24]. This shift is not merely a subtle geometric effect but has important implications for the exhaust handling capacity of W7-X: in particular, the most prominent qualitative feature is the appearance of an additional strike line located on the vertical target. The emergence of this secondary strike line highlights the strong sensitivity of power and particle exhaust to plasma conditions. This feature can be experimentally observed in the high- β programs. Fig. 12 displays another example of a combined ECRH and NBI improved confinement discharge, which reaches peak values of $\beta_{peak} \approx 5\%$. In this period of the discharge, clearly a second strike line on the vertical divertor target is directly observed (see red circle in Fig. 12) with mean heatflux values of $Q \approx 3 - 4 \ MW/m^2$.

Although there is a qualitative agreement of the position of the strike line on the divertor targets between calculations and measurements, the agreement of the quantitative predictions is inconsistent with observations. In Fig. 13 a comparison between calculations of the divertor target strike line width and SOL electron temperature profile using the EMC3 SOL modeling code is displayed for a variation of the particle diffusivity an highlights the inability to reliably model target heatflux and upstream profiles consistently. Although the a priori choice of the diffusivity can be tailored to match the observations in certain regions of the divertor and SOL, strong deviations are seen in other regions and it is generally not possible to match the experimental findings with with simple transport assumptions [25]. The agreement between experiment and simulations is improved if a spatially varying diffusivity is employed, but the use for a predictive assessment for, e.g., novel divertor design solutions remains a challenge [26]. One main influence not captured by the modeling approach is the effect of $E \times B$ drifts within the edge magnetic islands arising from the self-consistent radial plasma potential profile. Fig. 14(left) shows schematically the poloidal $E \times B$ drift pattern for the example of a lower divertor target module. It has been previously observed in W7-X that drifts create asymmetries between the top and bottom divertor [27] and alter the parallel flow distribution [28], particularly shifting the position of the flow stagnation point. The past experimental campaigns with the development of alternative plasma startup scenarios in reduced magnetic fields provide the possibility to quantitatively assess how SOL drift effects scale with field strength. In Fig. 14(right) the poloidal drift velocities in the standard magnetic configuration for two different field strengths are compared. In the power carrying layer just outside the last closed flux surface $(r - r_{LCFS} < 1 \text{ cm})$, the observed flow ratio $v_{\rm pol,1.8T}/v_{\rm pol,2.5T}=1.7$ is approx. 20% larger than the magnetic field ratio $2.5\,\mathrm{T}/1.8\,\mathrm{T}=1.4$, indicating a weak inverse scaling of E_r with B. These flows slightly shift the strike line position on the divertor target and the observed shifts are qualitatively consistent with the B-scaling of the flow velocity.

7. SUMMARY

The Wendelstein 7-X (W7-X) stellarator has recently completed two major experimental campaigns, OP 2.2 and OP 2.3, marking an important step toward demonstrating the viability of long-pulse, steady-state fusion operation. Instead of full recommissioning before each campaign, a new operational strategy was adopted that minimized downtime and allowed two extended phases of plasma research with only short maintenance in between. This required high reliability from all technical subsystems, which was successfully achieved with failure rates below 1%. Several key upgrades supported this progress, including the operation of a prototype high-power gyrotron delivering 1.3 MW of steady-state heating, a newly developed screw-type pellet injector for long-duration fueling, and advanced feedback control systems for radiation, power stabilization, and density regulation. Together, these

enhancements enabled a record discharge of 363 seconds with 1.8 GJ of injected heating energy, while maintaining safe divertor heat loads. In addition, innovative heating schemes allowed W7-X to explore high plasma-beta regimes, reaching unprecedented values of volume-averaged beta and demonstrating the impact of modified equilibria. Improved confinement scenarios were also realized through central density peaking, achieved either by neutral beam injection or pellet fueling, leading to record stellarator fusion triple products comparable to tokamaks, though at smaller scale. Long-pulse pellet fueling in particular opened the path to sustaining improved confinement over much longer durations. Finally, detailed studies of the divertor and scrape-off layer highlighted the influence of drifts and plasma currents on strike-line patterns and exhaust handling, showing both agreement and limitations in present modeling approaches. Collectively, these results confirm W7-X as the leading facility for steady-state stellarator research, advancing both the scientific understanding and the technical foundation needed for future fusion reactors.

ACKNOWLEDGEMENTS

This work has been carried out within the framework of the EUROfusion Consortium, funded by the European Union via the Euratom Research and Training Programme (Grant Agreement No. 101052200—EUROfusion). Views and opinions expressed are however those of the author(s) only and do not necessarily reflect those of the European Union or the European Commission. Neither the European Union nor the European Commission can be held responsible for them.

REFERENCES

- [1] S. Ponomarenko et al. *IEEE Electr. Device. L.* 45.12 (2024), pp. 2550–2553.
- [2] Steven J. Meitner et al. IEEE T. Plasma. Sci. 48.6, 1, SI (2020), pp. 1585–1590.
- [3] O. Grulke et al. *NUCLEAR FUSION* 64.11 (2024).
- [4] CD Beidler et al. Nucl. Fusion 41.12 (2001), pp. 1759–1766.
- [5] R. C. Wolf et al. *IEEE T. Plasma. Sci.* 44.9, 1, SI (2016), pp. 1466–1471.
- [6] M. Drevlak et al. *Nucl. Fusion* 54.7 (2014).
- [7] Nikolai B. Marushchenko et al. Ed. by E Poli, H Laqua, and J Oosterbeek. Vol. 203. EPJ Web of Conferences. Max Planck-Inst Plasma Phys. 2019.
- [8] M. N. A. Beurskens et al. *Nucl Fusion* 61.11 (2021).
- [9] A. Langenberg et al. Phys Plasmas 31.5 (2024).
- [10] O. P. Ford et al. Nucl Fusion 64.8 (2024).
- [11] S. Bannmann et al. *Nucl Fusion* 64.10 (2024).
- $[12] \quad S.\ A.\ Bozhenkov\ et\ al.\ \textit{Nucl Fusion}\ 60.6\ (2020).$
- [13] M. N. A. Beurskens et al. *Nucl Fusion* 62.1 (2022).
- [14] M. Wappl et al. Plasma Phys Control Fusion 67.7 (2025).
- [15] X. Litaudon et al. Nucl. Fusion 64.1 (2024).
- [16] P. Xanthopoulos et al. Phys. Rev. Lett. 99 (3 2007).
- [17] J A Alcusón et al. Plasma Phys Control Fusion 62.3 (2020).
- [18] J-P. Baehner et al. *J Plasma Phys* 87.3 (2021).
- [19] Th. Wegner et al. Nucl Fusion 60.12 (2020).
- [20] J. H. E. Proll et al. Phys. Rev. Lett. 108 (24 2012).
- [21] P. Helander et al. Phys. Rev. Lett. 118 (15 2017).
- [22] X. Litaudon et al. this 30th IAEA FEC (2025).
- [23] Y. Gao et al. Nucl Fusion 59.6 (2019).
- [24] A. Knieps et al. *Nucl Fusion* 62.2 (2022).
- [25] David Bold et al. Nucl Fusion 62.10 (2022).
- [26] David Bold et al. Nucl Fusion 64.12 (2024).
- [27] K. C. Hammond et al. *Plasma Phys Control Fusion* 61.12 (2019).
- [28] D. M. Kriete et al. Nucl Fusion 63.2 (2023).